ARTICLE IN PRESS

Available online at www.sciencedirect.com

ScienceDirect

Advances in Space Research xxx (2016) xxx–xxx

ADVANCES IN SPACE RESEARCH (a COSPAR publication)

www.elsevier.com/locate/asr

# Incremental inverse kinematics based vision servo for autonomous robotic capture of non-cooperative space debris

Gangqi Dong, Z.H. Zhu *

*Department of Earth and Space Science and Engineering, York University, 4700 Keele Street, Toronto, Ontario M3J 1P3, Canada*

Received 31 October 2015; received in revised form 31 December 2015; accepted 12 January 2016

**Abstract**

This paper proposed a new incremental inverse kinematics based vision servo approach for robotic manipulators to capture a non-cooperative target autonomously. The target's pose and motion are estimated by a vision system using integrated photogrammetry and EKF algorithm. Based on the estimated pose and motion of the target, the instantaneous desired position of the end-effector is predicted by inverse kinematics and the robotic manipulator is moved incrementally from its current configuration subject to the joint speed limits. This approach effectively eliminates the multiple solutions in the inverse kinematics and increases the robustness of the control algorithm. The proposed approach is validated by a hardware-in-the-loop simulation, where the pose and motion of the non-cooperative target is estimated by a real vision system. The simulation results demonstrate the effectiveness and robustness of the proposed estimation approach for the target and the incremental control strategy for the robotic manipulator.


*Keywords:* Visual servo; Autonomous capture; Non-cooperative target; Space debris; Active debris removal; Space robotic manipulator

## 1. Introduction

The increasing population of space debris in low and geo-stationary Earth orbits severely threats the safety of orbiting satellites and the long-term sustainability of space activities (Jankovic et al., 2015). To address the threat on a global base, the Inter-Agency Space Debris Coordination Committee (IADC) has suggested that certain remediation measures must be taken to stabilize the increasing trend of space debris population, for instance, by active debris removal (ADR) of a few large space debris per year from some crowded altitudes and inclinations of orbits (Liou, 2011). Numerous debris removal technologies have been proposed and investigated, such as the robotic debris removal (Jankovic et al., 2015), hybrid propulsion module (DeLuca et al., 2013), harpoon technology (Dudziak et al., 2015), and concepts considering end-of-mission self-deorbit by electrodynamic tethers (Zhong and Zhu, 2013), etc. Due to the similarity between the robotic on-orbit servicing (OOS) and ADR missions, the concept of autonomous ADR missions using space robotic manipulators is appealing in terms of technology readiness level. Although numerous human-in-the-loop OOS missions involving robotic captures of spacecraft were successfully performed (Yoshida, 2009), a fully autonomous robotic capture in space, especially considering non-cooperative objects is still an open subject facing enormous technical challenges (Flores-Abad et al., 2014). Recently, a preliminary concept design of guidance, navigation and control architecture to enable a safe and fuel-efficient capture of a non-cooperative target had been proposed (Jankovic et al., 2015), where the attention was focused on the close range autonomous rendezvous and proximity maneuver. In this paper, we focus

* Corresponding author. Tel.: +1 416 7362100x77729.
*E-mail address:* gzhu@yorku.ca (Z.H. Zhu).

http://dx.doi.org/10.1016/j.asr.2016.01.011
0273-1177/

Please cite this article in press as: Dong, G., Zhu, Z.H. Incremental inverse kinematics based vision servo for autonomous robotic capture of non-cooperative space debris. Adv. Space Res. (2016), http://dx.doi.org/10.1016/j.asr.2016.01.011

on the autonomous capture of a non-cooperative target by a robotic manipulator after the orbit maneuver being completed.

One of the most challenging tasks in the autonomous capture of a non-cooperative target is the identification of target's kinematic state. Considering the non-cooperative nature, the non-intrusive vision based filtering methods have been extensively adopted in the pose estimation of target (Aghili, 2012; Chen, 2012; Gasbarri et al., 2014; Janabi-Sharifi and Marey, 2010; Sabatini et al., 2013). Once the position and velocity of a target are obtained, an effective controller is required to control a robotic manipulator to capture the target autonomously. Ideally, the interception point between trajectories of the target and the end-effector in capture scenarios should be used as the desired position of the end-effector in control (Liu et al., 2015). However, due to the non-cooperative nature, the trajectory of target is unknown in advance and the determination of the interception point becomes a challenging task. The task is further complicated by the fact that the velocity of the end-effector is related to the configuration (joint angles) of robotic manipulator, which is time-variant and nonlinear. Thus, the interception point is also subject to the variation of interception time. In order to address this challenge, a kinematics based incremental control strategy for the robotic manipulator is proposed and examined in this work. Since the capture process of a space debris is relatively slow, it is more intuitive to regard the joint position (joint angles) as control input to gain higher control reliability instead of velocity or acceleration. The paper is organized as follows. Followed by this brief introduction, Section 2 is dedicated to the vision based kinematic state estimation of a non-cooperative target by an integrated photogrammetry and extended Kalman filter approach. A kinematics based incremental controller for the robotic manipulator is then presented in Section 3. Section 4 is dedicated to the validation by hardware-in-the-loop simulation and discussion. Finally, Section 5 concludes the paper.

## 2. Vision based kinematic identification of non-cooperative target

Consider a robotic manipulator system shown in Fig. 1. Assume a global frame is attached to the fixed part of the robotic manipulator, a camera frame is fixed to the center of image plane, and a target frame to the center of rotation of the target, respectively. The transformation between the global and the camera frame can be easily obtained according to the system configuration. The pose of a target can be described with respect to (w.r.t.) the camera frame, such as, $\{x_{To}, y_{To}, z_{To}, \theta_x, \theta_y, \theta_z\}^T$, where $\{x_{To}, y_{To}, z_{To}\}^T$ is the origin of the target frame in the camera frame and $\{\theta_x, \theta_y, \theta_z\}^T$ are the Euler angles of the target frame w.r.t. the camera frame.

Accordingly, an augmented homogeneous transformation between the target and the camera frame can be written as

$$\begin{Bmatrix} x_C \\ y_C \\ z_C \\ 1 \end{Bmatrix} = \begin{bmatrix} & \mathbf{R}_{TC} & & x_{To} \\ & & & y_{To} \\ & & & z_{To} \\ 0 & 0 & 0 & 1 \end{bmatrix} \begin{Bmatrix} x_T \\ y_T \\ z_T \\ 1 \end{Bmatrix} \tag{1}$$

where $\mathbf{R}_{TC}$ denotes the rotational matrix from the target to the camera frame formed by the composition of trigonometric functions of Euler angles, $\{x_T, y_T, z_T\}^T$ denote the coordinates of a feature point on the target in the target frame and $\{x_C, y_C, z_C\}^T$ denote the corresponding coordinates of the same feature point in the camera frame.

Consider a pinhole camera with a focal length $f$. By assuming the $y$-axis of the camera frame pointing toward the target, the feature point is projected onto the image plane by

$$\begin{Bmatrix} x_m \\ z_m \end{Bmatrix} = -\frac{f}{y_C - f} \begin{Bmatrix} x_C \\ z_C \end{Bmatrix} \tag{2}$$

where $\{x_m, z_m\}^T$ denotes the measurable image coordinates.

Substituting Eq. (1) into (2) yields two independent equations for one feature point, which contains six unknowns: $\{x_{To}, y_{To}, z_{To}, \theta_x, \theta_y, \theta_z\}^T$. Theoretically, one needs at least three feature points to solve for the six unknowns. However, four feature points are widely adopted in literature to avoid the ambiguity and increase the robustness of algorithm (Dong and Zhu, 2015). Consequently, there will be eight equations with six unknowns, which can be solved by an iterative least square approach with an initial guess. The pose estimation of a non-cooperative target by the photogrammetry is a Markov process based on the current measurement, which is prone to the measurement noise. Moreover, the computational time of photogrammetry may vary widely due to the initial guess used in the algorithm at each time instant. As a result, the system sampling time interval may be affected, which is undesirable for real-time control. Another issue of the photogrammetry is that it does not solve for motion directly, which is an important control parameter in capturing the target by a robotic manipulator autonomously in a dynamic scenario. To address these challenges, an integrated photogrammetry and extended Kalman filter (EKF) is presented as follows.

Define the system variable vector as

$$\mathbf{X} = \{x_{To}, \dot{x}_{To}, y_{To}, \dot{y}_{To}, z_{To}, \dot{z}_{To}, \theta_x, \dot{\theta}_x, \theta_y, \dot{\theta}_y, \theta_z, \dot{\theta}_z\}^T$$

Assume the target motion can be approximated as a linear motion within each sampling time interval $t_s$ if it is sufficiently small. Thus, the system model of the target can be expressed as

$$\mathbf{X}_k = \mathbf{A}\mathbf{X}_{k-1} + \mathbf{B}\boldsymbol{\omega}_{k-1} \tag{3}$$

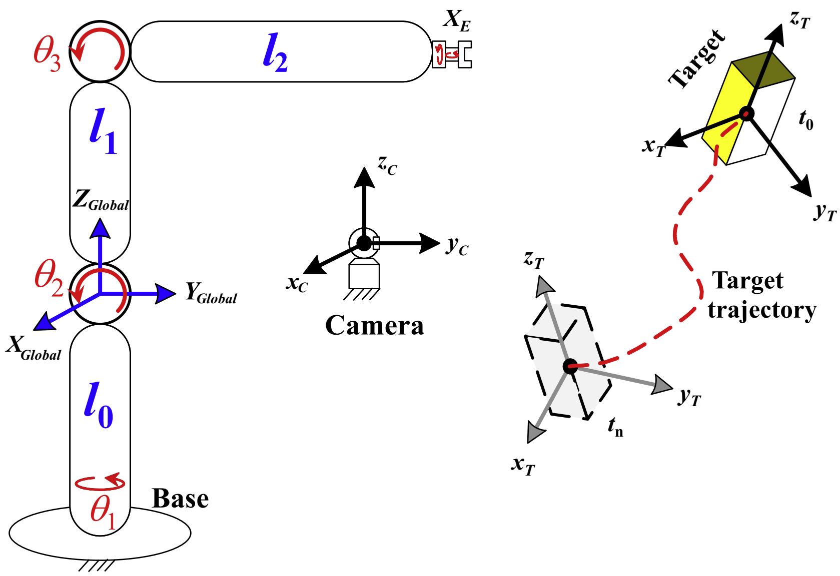


Fig. 1. Illustration of different coordinate systems.

where the subscripts $k$ and $k-1$ denotes the current and previous states respectively, $\boldsymbol{\omega} = \{\ddot{x}_{To}, \ddot{y}_{To}, \ddot{z}_{To}, \ddot{\theta}_x, \ddot{\theta}_y, \ddot{\theta}_z\}^T$ is the acceleration vector that is considered as the process noise subject to the normal distribution with zero mean and covariance matrix $\mathbf{Q}$, and the coefficient matrices $\mathbf{A}$ and $\mathbf{B}$ are defined as

$$\mathbf{A} = diag[A \quad A \quad A \quad A \quad A \quad A], \quad A = \begin{bmatrix} 1 & t_s \\ 0 & 1 \end{bmatrix} \tag{4}$$

$$\mathbf{B} = diag[B \quad B \quad B \quad B \quad B \quad B], \quad B = \begin{Bmatrix} t_s^2/2 \\ t_s \end{Bmatrix} \tag{5}$$

Based on the pinhole camera from Eq. (2), the measurement model is defined as,

$$\mathbf{Z}_k = \mathbf{h}(\mathbf{X}_k) + \boldsymbol{\mu}_k \tag{6}$$

where $\mathbf{h}(\mathbf{X}) = -\dfrac{f}{y_C - f}\begin{Bmatrix} x_C \\ z_C \end{Bmatrix}$ is an equation vector for one feature point, $\boldsymbol{\mu}$ stands for the measurement noise that obeys the normal distribution with zero mean and covariance matrix $\mathbf{R}$, and $\mathbf{Z}$ is the real measurement vector of feature points.

Once the system and measurement models are derived, the EKF is applied to estimate the kinematic state of the target, such that,

$$\begin{cases} \mathbf{X}_{k|k-1} = \mathbf{A}\mathbf{X}_{k-1|k-1} \\ \mathbf{P}_{k|k-1} = \mathbf{A}\mathbf{P}_{k-1|k-1}\mathbf{A}^T + \mathbf{B}\mathbf{Q}\mathbf{B}^T \\ \mathbf{K}_g = \mathbf{P}_{k|k-1}\mathbf{H}^T[\mathbf{H}\mathbf{P}_{k|k-1}\mathbf{H}^T + \mathbf{R}]^{-1} \\ \mathbf{X}_{k|k} = \mathbf{X}_{k|k-1} + \mathbf{K}_g[\mathbf{Z}_k - \mathbf{h}(\mathbf{X}_{k|k-1})] \\ \mathbf{P}_{k|k} = \mathbf{P}_{k|k-1} - \mathbf{K}_g\mathbf{H}\mathbf{P}_{k|k-1} \end{cases} \tag{7}$$

where $\mathbf{H}$ is the Jacobian matrix of the measurement model, $\mathbf{P}$ is the covariance matrix of the system variable, and $\mathbf{K}_g$ is the Kalman gain.

As well known, the input of EKF includes initial conditions known in advance and measurements observed over time. Since initial conditions of a non-cooperative target are unknown, inappropriate initial guess may lead to poor performance of the EKF. Therefore, we initialized the EKF by the photogrammetry in order to improve the performance as well as accelerate the convergence rate of the EKF.

## 3. Kinematics based incremental control strategy

The forward kinematics of a robotic manipulator defines the position and velocity of the end-effector in terms of the corresponding joint variables, such that

$$\mathbf{X}_E = \mathbf{f}(\boldsymbol{\Theta}) \tag{8}$$

$$\dot{\mathbf{X}}_E = \mathbf{J}\dot{\boldsymbol{\Theta}} \tag{9}$$

where $\mathbf{X}_E \in \mathbf{R}^m$ is the position of the end-effector in the Cartesian space, $\boldsymbol{\Theta} \in \mathbf{R}^n$ is the generalized joint variable vector in the joint space, the overhead dot denotes the time derivative and $\mathbf{J}$ is the Jacobian matrix of the robotic manipulator defined by $\mathbf{J} = \partial\mathbf{f}/\partial\boldsymbol{\Theta}$.

In order to perform the capture task, one has to determine the joint angles by the inverse kinematics of robotic manipulator based on the information of the end-effector. The inverse of Eq. (8) may have multiple solutions due to system redundancy and periodicity of trigonometric functions. In order to obtain unique solution, physical limits or other extra constraints may have to be imposed. Generally, the complete inverse of Eq. (9) is composed by two parts, the particular solution and the null space solution. The particular solution can be obtained based on the pseudo inverse of the Jacobian matrix, denoted by $\mathbf{J}^\dagger$. Although the pseudo-inverse of the Jacobian matrix can be calculated by using the singular value decomposition, the computational load is relatively heavy. In many robotic applications, the Jacobian matrix is assumed to have full row rank, and the pseudo-inverse is replaced by the right inverse, such that, $\mathbf{J}^{\dagger} = \mathbf{J}^{T}(\mathbf{J}\mathbf{J}^{T})^{-1}$. Thus the complete solution for the inverse of Eq. (9) is written as

$$\dot{\mathbf{\Theta}} = J^{\dagger}\dot{\mathbf{X}}_E + (\mathbf{I} - \mathbf{J}^{\dagger}\mathbf{J})\xi \tag{10}$$

where $\mathbf{I}$ denotes the identity matrix and $\xi$ is an arbitrary vector that projected onto the null space of the Jacobian. Therefore, by careful selection of this vector, additional kinematic objectives can be achieved if the kinematic redundancy exists.

Once the position and velocity of the target w.r.t. the camera frame is obtained in Section 2, we may easily transform them to the global frame by the homogeneous transformation, such that

$$\begin{pmatrix} \mathbf{X}_T \\ 1 \end{pmatrix} = \mathbf{T}\begin{pmatrix} {}^{C}\mathbf{X}_T \\ 1 \end{pmatrix} \tag{11}$$

$$\begin{pmatrix} \dot{\mathbf{X}}_T \\ 1 \end{pmatrix} = \mathbf{T}\begin{pmatrix} {}^{C}\dot{\mathbf{X}}_T \\ 1 \end{pmatrix} + \dot{\mathbf{T}}\begin{pmatrix} {}^{C}\mathbf{X}_T \\ 1 \end{pmatrix} \tag{12}$$

where $\mathbf{X}_T, \dot{\mathbf{X}}_T$ and ${}^{C}\mathbf{X}_T, {}^{C}\dot{\mathbf{X}}_T$ stand for the target position and velocity w.r.t. the global and camera frame respectively, $\mathbf{T}$ denotes the Denavit–Hartenberg transformation matrix from the camera frame to the global frame (Denavit and Hartenberg, 1955), which can be easily obtained according to the geometric configuration of the system.

In the eye-to-hand configuration, the camera is stationary in the global frame. Therefore, the transformation matrix between the two camera and global frames will be time-invariant and the time derivative of the transformation matrix is zero matrix, such that, $\dot{\mathbf{T}} = \mathbf{0}$ in Eq. (12).

Once the position and velocity of the target in the global frame is obtained, the position of the target in the next moment can be estimated by

$$\mathbf{X}_{T'} = \mathbf{X}_T + \dot{\mathbf{X}}_T t_s \tag{13}$$

In order to make a capture, the most straightforward way for the end-effector to approach the target is directly towards it if the velocity of the target is relatively small compare to the robotic manipulator. Accordingly, the instantaneous velocity of the end-effector in the Cartesian space should be along with the vector defined by $\mathbf{X}_{T'} - \mathbf{X}_E$.

Denote the unit vector of $\mathbf{X}_{T'} - \mathbf{X}_E$ as

$$\mathbf{n}_{ET'} = \frac{\mathbf{X}_{T'} - \mathbf{X}_E}{\|\mathbf{X}_{T'} - \mathbf{X}_E\|} \tag{14}$$

Define the scale factor of the instantaneous velocity as $\lambda > 0$, so that the instantaneous velocity of the end-effector can be written as

$$\dot{\mathbf{X}}_E = \lambda\mathbf{n}_{ET'} \tag{15}$$

For the sake of simplicity, assume $\boldsymbol{\xi} = \mathbf{0}$ in Eq. (10). Then, substituting Eq. (15) into Eq. (10) leads to

$$\dot{\mathbf{\Theta}} = \lambda\mathbf{J}^{\dagger}\mathbf{n}_{ET'} \tag{16}$$

Let $\dot{\theta}_i, p_{ij}$ and $n_{ET'j}$ be the elements of $\dot{\mathbf{\Theta}}, \mathbf{J}^{\dagger}$ and $\mathbf{n}_{ET'}$, respectively. Then, Eq. (16) can be replaced by $n$ scalar equations, such that

$$\dot{\theta}_i = \lambda\sum_{j=1}^{m} p_{ij} n_{ET'j}, \quad i = 1, 2, \cdots, n. \tag{17}$$

Due to the physical limit of the joint actuators and the transmission mechanisms, the motion of the robotic manipulator is subject to the joint velocity limit, denoted by $\dot{\mathbf{\Theta}}_{\max} = (\dot{\theta}_{\max 1}, \dot{\theta}_{\max 2}, \cdots, \dot{\theta}_{\max n})^{T}$. Assume the joint velocity has the same limit in both positive and negative directions, then the right side of equations in Eq. (17) is bounded by the closed interval $[-\dot{\theta}_{\max i}, \dot{\theta}_{\max i}]$, respectively, such that

$$-\dot{\theta}_{\max i} \leqslant \lambda\sum_{j=1}^{m} p_{ij} n_{ET'j} \leqslant \dot{\theta}_{\max i}, \quad i = 1, 2, \cdots, n. \tag{18}$$

Solving inequalities in Eq. (18) for $\lambda$ yields $n$ sets of scale factor $\lambda_i$. Then, the maximum scale factor of the instantaneous velocity can be found by taking the intersection of each solution, such as, $\lambda_{\max} = \max[\lambda_1 \cap \lambda_2 \cap \cdots \cap \lambda_n]$. By substituting $\lambda_{\max}$ into Eq. (16), we obtain the equivalent instantaneous joint velocity of the robotic manipulator, denoted by $\dot{\mathbf{\Theta}}_{\upsilon}$. Accordingly, the incremental joint angle control input for the robotic manipulator in the next moment, which will drive the end-effector directly towards the target, can be defined as,

$$\Delta\mathbf{\Theta} = \dot{\mathbf{\Theta}}_{\upsilon} t_s \tag{19}$$

The control input of the robotic manipulator could be $\mathbf{\Theta} + \Delta\mathbf{\Theta}$ if the control is achieved by absolute joint angles. After the end-effector moving towards the target by an increment $\Delta\mathbf{X}_E = \mathbf{J}\Delta\mathbf{\Theta}$, the procedure defined in Eqs. (13)–(19) is repeated for the next sampling time. A capture will be done once the position error between the end-effector and the target is within a pre-defined tolerance, denoted by $\boldsymbol{\varepsilon} \in \mathbf{R}^{m}$, such that,

$$|\mathbf{X}_E - \mathbf{X}_T| < \boldsymbol{\varepsilon} \tag{20}$$

## 4. Validation by hardware-in-the-loop simulation

The proposed kinematics based incremental control strategy is validated by hardware-in-the-loop simulation. The robotic manipulator is assumed to consist of three rigid links and three revolute joints. The visual control is done by an eye-to-hand configuration. The link length and the joint velocity limits of the manipulator are given in Table 1, based on our previous work (Dong and Zhu, 2015).

The joint angles are measured from their home positions $\theta_1 = 0^\circ, \theta_2 = 90^\circ, \theta_3 = 0^\circ$, as illustrated in Fig. 1. The global frame is located to the center of the second joint and fixed in the inertia space, and the camera frame is attached

Table 1
Physical properties of the robotic manipulator.

| Parameter | Value |
|---|---|
| $l_0$ | 0.1778 m |
| $l_1$ | 0.454025 m |
| $l_2$ | 0.4445 m |
| $\dot{\theta}_{\max 1}$ | 10.304 rad/s |
| $\dot{\theta}_{\max 2}$ | 0.412 rad/s |
| $\dot{\theta}_{\max 3}$ | 0.412 rad/s |

to the center of camera's image plane, which coincides with the home position of the end-effector for simplicity. Accordingly, the Jacobian matrix of the robotic manipulator can be easily obtained. In order to simplify the calculation and reduce the computational cost in our case, the kinematic singularity of the robotic manipulator is physically avoided by limiting its workspace. Then, the pseudo-inverse of the Jacobian, which will be full rank, can be calculated simply by $\mathbf{J}^{\dagger} = \mathbf{J}^{-1}$.

The non-cooperative target is independently moving along a trajectory within the 3D workspace of the robotic manipulator. Its motion and trajectory are unknown in advance and must be estimated by the vision system. Fig. 2 shows the estimated position $\mathbf{X}_T = (x_T, y_T, z_T)^T$ and velocity $\dot{\mathbf{X}}_T = (\dot{x}_T, \dot{y}_T, \dot{z}_T)^T$ of the target by the eye-to-hand camera using the integrated approach presented in Section 2 w.r.t. the global frame. These profiles are input to the controller to calculate the incremental control input for the robotic manipulator.

The control input to the robotic manipulator in our case is the incremental joint angles. As shown clearly in Fig. 3, the calculated instantaneous joint velocities $\dot{\theta}_2$ and $\dot{\theta}_3$ reach the physical limits listed in Table 1 in certain periods, respectively. In general, the calculated instantaneous joint velocities $\dot{\mathbf{\Theta}}_v$ are quite smooth because the estimated position and velocity of the non-cooperative target in the global frame are relatively smooth. However, the control inputs $\Delta\mathbf{\Theta}$ in the Fig. 4 show isolated outliers from time to time although the overall trends are smooth. This is because the sampling time used in the controller is dictated by the image processing time, which varies from time to time. Accordingly, the incremental control input $\Delta\mathbf{\Theta}$ obtained by Eq. (19) is affected by the time-varying sampling time. If simulated target motion and velocity are used, there will be no outliers in the incremental control input. This indicates it is important to keep the sampling time constant in real implementation of visual servo control algorithm of robotic manipulator.

The simulation results of an autonomous capture by the robotic manipulator are shown in Fig. 4. The solid lines and circles denote the trajectories of the target and the end-effector respectively. The robotic manipulator is at the home position initially. By defining $\boldsymbol{\varepsilon} = (10^{-3}, 10^{-3}, 10^{-3})^T$ meters in Eq. (20), a capture is made at about

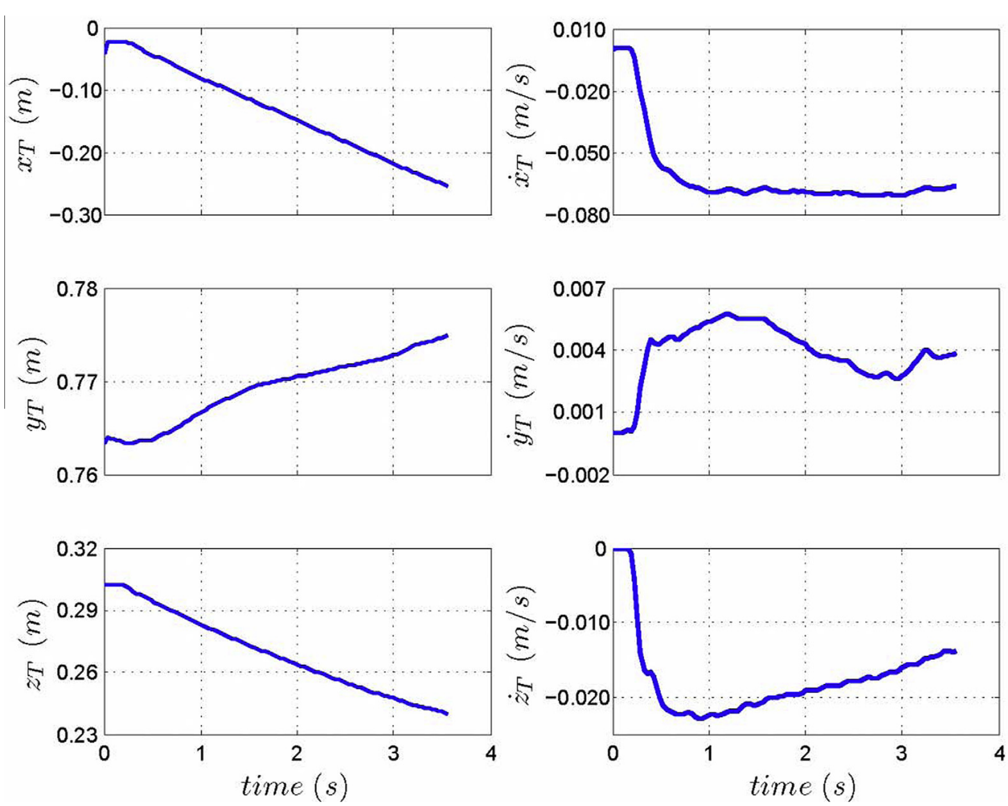


Fig. 2. Estimated position and velocity of the non-cooperative target in global frame.

Please cite this article in press as: Dong, G., Zhu, Z.H. Incremental inverse kinematics based vision servo for autonomous robotic capture of non-cooperative space debris. Adv. Space Res. (2016), http://dx.doi.org/10.1016/j.asr.2016.01.011

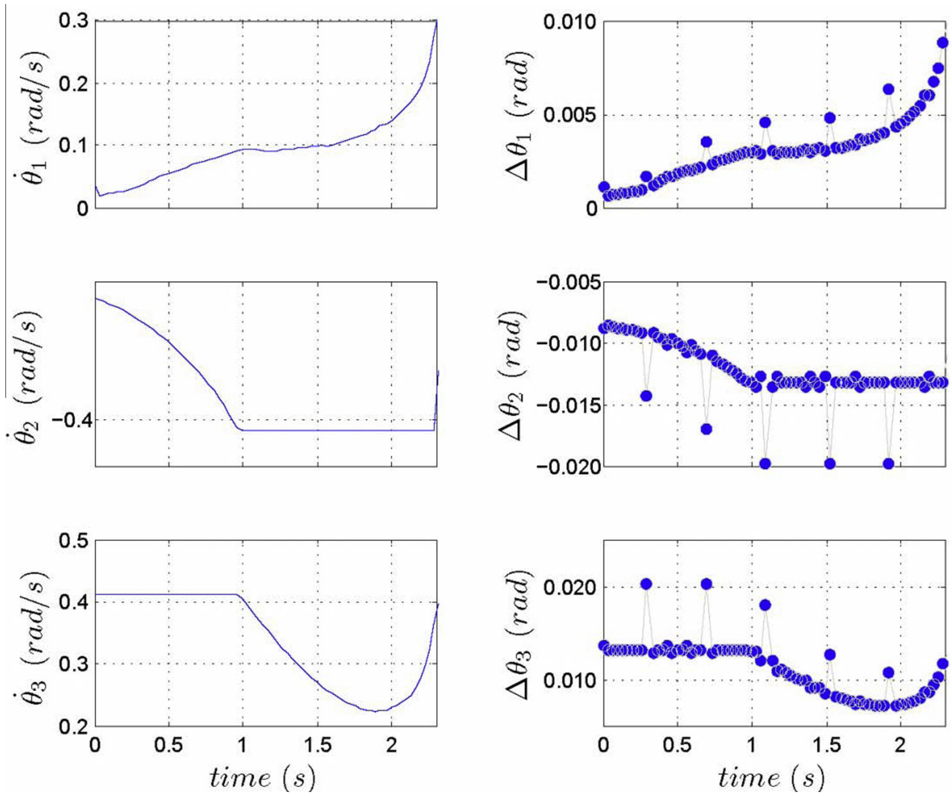


Fig. 3. Instantaneous joint velocity and incremental control input of the robotic manipulator.

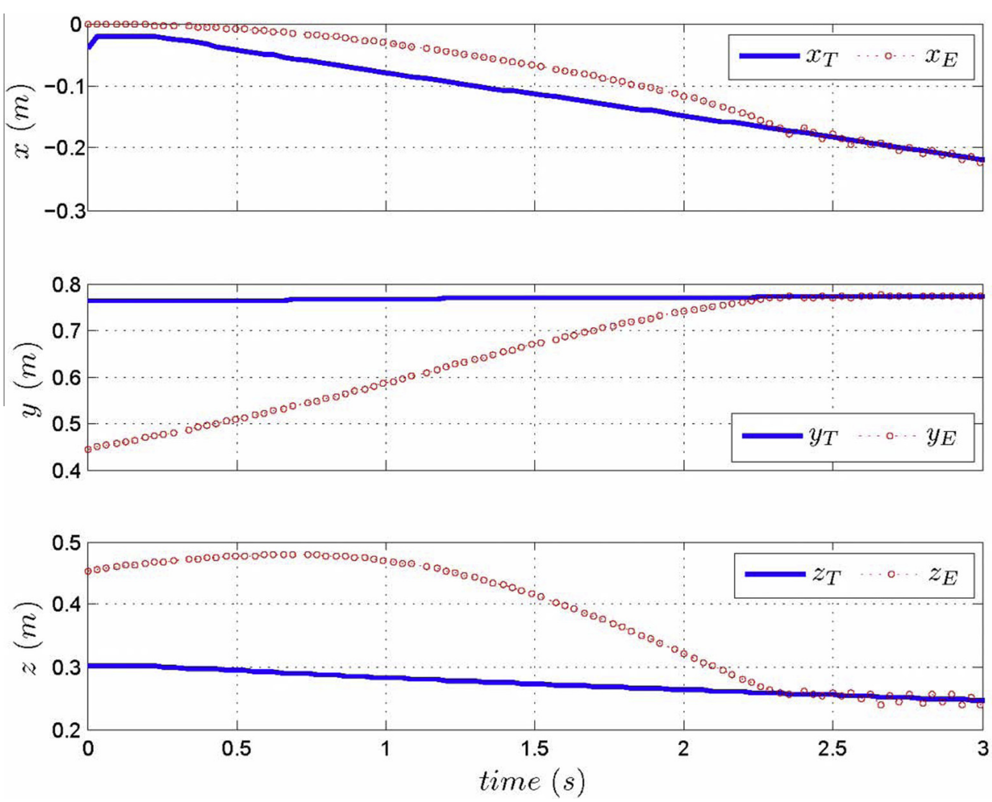


Fig. 4. Position of the target and the end-effector.

Please cite this article in press as: Dong, G., Zhu, Z.H. Incremental inverse kinematics based vision servo for autonomous robotic capture of non-cooperative space debris. Adv. Space Res. (2016), http://dx.doi.org/10.1016/j.asr.2016.01.011

2.3 s once the capture criteria is achieved. The position profiles of the end-effector in Fig. 4 are smooth and approximately monotonic, although there are some outliers in the incremental control input. This is generally preferred in the operation of robotic manipulators. The simulation results shown in Figs. 3 and 4 demonstrate the proposed kinematics based incremental control strategy is effective and efficient.

## 5. Conclusions

This paper proposed a new vision-based incremental kinematic control strategy for a robotic manipulator to perform autonomous capture of a non-cooperative target. The target's pose and motion are estimated visually by an integrated photogrammetry and EKF approach. Based on the input of target's pose and motion, the forward kinematics of robot manipulator is inversed in an incremental form where the robotic manipulator moves by increments from its current configuration. By adopting this approach, the multiple-solution problem of the inverse kinematics has been avoided. Since the velocity of the end-effector in Cartesian space in the current approach is always pointing to the target in the next moment, the possibility of losing track of the target by the vision system is greatly reduced. The proposed approach is validated by a hardware-in-the-loop simulation, where the pose and motion of the non-cooperative target is estimated by a real vision system. The simulation results of capture demonstrated proposed kinematics based incremental control strategy is effective and efficient.

## Acknowledgements

This work is supported by the Natural Sciences and Engineering Research Council of Canada.

## References

Aghili, F., 2012. A prediction and motion-planning scheme for visually guided robotic capturing of free-floating tumbling objects with uncertain dynamics. IEEE Trans. Rob. 28, 634–649.

Chen, S.Y., 2012. Kalman filter for robot vision: a survey. IEEE Trans. Ind. Electron. 59, 4409–4420.

DeLuca, L.T., Bernelli, F., Maggi, F., et al., 2013. Active space debris removal by a hybrid propulsion module. Acta Astronaut. 91, 20–33.

Denavit, J., Hartenberg, R.S., 1955. A kinematic notation for lower-pair mechanisms based on matrices. Trans. ASME J. Appl. Mech. 23, 215–221.

Dong, G., Zhu, Z.H., 2015. Position-based visual servo control of autonomous robotic manipulators. Acta Astronaut. 115, 291–302.

Dudziak, R., Tuttle, S., Barraclough, S., 2015. Harpoon technology development for the active removal of space debris. Adv. Space Res. 56, 509–527.

Flores-Abad, A., Ma, O., Pham, K., Ulrich, S., 2014. A review of space robotics technologies for on-orbit servicing. Prog. Aerospace Sci. 68, 1–26.

Gasbarri, P., Sabatini, M., Palmerini, G.B., 2014. Ground tests for vision based determination and control of formation flying spacecraft trajectories. Acta Astronaut. 102, 378–391.

Janabi-Sharifi, F., Marey, M., 2010. A Kalman-filter-based method for pose estimation in visual servoing. IEEE Trans. Rob. 26, 939–947.

Jankovic, M., Paul, J., Kirchner, F., 2015. GNC architecture for autonomous robotic capture of a non-cooperative target: preliminary concept design. Adv. Space Res.

Liou, J.C., 2011. An active debris removal parametric study for LEO environment remediation. Adv. Space Res. 47, 1865–1876.

Liu, X.F., Li, H.Q., Chen, Y.J., Cai, G.P., Wang, X., 2015. Dynamics and control of capture of a floating rigid body by a spacecraft robotic arm. Multibody Syst. Dyn. 33, 315–332.

Sabatini, M., Monti, R., Gasbarri, P., Palmerini, G.B., 2013. Adaptive and robust algorithms and tests for visual-based navigation of a space robotic manipulator. Acta Astronaut. 83, 65–84.

Yoshida, K., 2009. Achievements in space robotics expanding the horizons of service and exploration. IEEE Rob. Autom. Mag. 16, 20–28.

Zhong, R., Zhu, Z.H., 2013. Dynamics of nanosatellite deorbit by bare electrodynamic tether in low earth orbit. J. Spacecraft Rockets 50, 691–700.

Please cite this article in press as: Dong, G., Zhu, Z.H. Incremental inverse kinematics based vision servo for autonomous robotic capture of non-cooperative space debris. Adv. Space Res. (2016), http://dx.doi.org/10.1016/j.asr.2016.01.011